DOI 10.5012/bkcs.2011.32.4.1331

Annealing Temperature Dependence on the Physicochemical Properties of Copper Oxide Thin Films

J. Y. Park,[†] T. H. Kwon,[‡] S. W. Koh,[§] and Y. C. Kang[†,*]

Department of [†]Chemistry, [‡]Electronics and [§]Division of Mechanical Engineering, Pukyong National University, Busan 608-737, Korea. [*]E-mail: yckang@pknu.ac.kr
Received February 1, 2011, Accepted February 22, 2011

We report the results of the characterization of Cu oxide thin films deposited by radio frequency (r.f.) magnetron sputtering at different annealing temperatures. The deposited Cu oxide thin films were investigated by scanning electron microscopy, spectroscopic ellipsometry, X-ray diffraction, atomic force microscopy, X-ray photoelectron spectroscopy, and contact angle measurements. The thickness of the films was about 180 nm and the monoclinic CuO phase was detected. The CuO_2 and $Cu(OH)_2$ phases were grown as amorphous phase and the ratio of the three phases were independent on the annealing temperature. The surface of Cu oxide films changed from hydrophilic to hydrophobic as the annealing temperature increased. This phenomenon is due to the increase of the surface roughness. The direct optical band gap was also obtained and laid in the range between 2.36 and 3.06 eV.

Key Words : Copper oxide, Wettability, Band gap, Crystallinity

Introduction

The Cu oxide has two crystalline phases: Cu_2O (cuprous oxide or cuprite) and CuO (cupric oxide or tenorite). Cu_2O is a p-type semiconductor with band gap of 2.0-2.6 eV[1-3] and cubic structure. Otherwise CuO has a relatively low band gap (1.3-2.1 eV[4,5]) and is occasionally considered as an n-type semiconductor and monoclinic structure. The application fields of those are slightly different because of the distinct characteristics between cuprous and cupric oxide. Copper oxides were used for gas sensors for hydrogen[6] and volatile organic compounds,[7] catalysis,[8] and specially, cuprous oxide films were intensively researched in device applications such as photovoltaic solar cell,[9] photoelectrochemical cell,[10,11] and electrochromic coatings.[12]

A wide range of deposition techniques such as chemical vapor deposition,[13] electrodeposition,[14] thermal evaporation,[15] sol-gel techniques,[16] spray pyrolysis,[17] pulsed laser deposition,[18] and plasma based ion implantation and deposition[19] have been used to prepare metal oxide films including Cu oxide films. The physical and chemical properties of the films are affected by the deposition method and its conditions. In addition, it can also be influenced on the electrical properties, for example, band gap and these large variations can make Cu oxide films suitable for many applications. Among various deposition methods, reactive radio frequency (r.f.) magnetron sputtering is the most commonly used method to synthesize films with splendid quality. Figueiredo *et al.* have reported that the effect of post-annealing of Cu oxide thin films obtained by thermal oxidation and revealed that the crystallinity and grain size of thin films were dependent on the post-annealing temperature.[20] The influence of other parameters such as r.f. power and oxygen flow rate on Cu oxide thin films prepared by reactive magnetron sputtering was studied by Ogwu *et al.*.[21] However in our knowledge, annealing effect on the Cu oxide thin films during deposition by r.f. sputtering is rare. In this study, Cu oxide thin films were prepared by reactive r.f. magnetron sputtering method on p-type Si(100) substrate at various annealing temperatures. The substrates were annealed between room temperature to 350 °C during deposition. The effect of annealing temperature on the structure, physical, chemical, and wetting properties of the copper oxide thin films was investigated.

Experimental Section

Copper oxide thin films were synthesized with metallic Cu target on p-type Si(100) wafer, which was cleaned by the HF cleaning process to remove the surface oxide, applying r.f. (13.56 MHz) magnetron sputtering. The deposition chamber was evacuated using a rotary vane pump and a turbo molecular pump to reach 1.0×10^{-7} Torr of base pressure. Highly pure argon (99.99%) for sputtering Cu target and oxygen (99.99%) for reactive gases were used for Cu oxide deposition. The introduced gases were controlled by mass flow controllers, separately. The total gas flux was kept at 20 sccm and the mixing ratio (O_2/O_2 + Ar) was 0.5. In order to clean the Cu target and stabilize the plasma, pre-sputtering was performed while the substrate was shielded for 1 hr. The deposition of Cu oxide thin films was performed with a r.f. power of 40 W for 3 hrs after pre-sputtering process and the working pressure was 50 ± 0.5 mTorr. In our work, Cu oxide thin films were obtained at different annealing temperatures from room temperature to 300 °C.

The thickness of the Cu oxide thin films was measured by cross-sectional images of field emission scanning electron microscopy (FESEM, JEOL JSM-6700F, Japan). The images were obtained with a high voltage of 15 kV and 9 ~ 10 mA

of beam current and the film surface was coated with OsO_4 before introducing it into the analysis chamber for better resolution. Another method to analyze the thickness of films was spectroscopic ellipsometry (SE, J. A. Woollam M-2000D, USA) for cross checking. The D_2 and quartz tungsten halogen sources were adopted to obtain the spectra in the wavelength range of 193 to 1000 nm. The beam size was 2 mm and the incident angle was 75°. In addition, the SE data were used to determine the surface roughness and direct band gap. The surface morphology of Cu oxide thin films was investigated using an atomic force microscopy (AFM, Veeco Multimode digital Instruments Nanoscope IIIα, USA) in contact mode. The scan size, scan rate, and tip velocity was 2.00 × 2.00 μm^2, 1.97 Hz, and 7.88 μm/s, respectively. The root mean square (RMS) values were used to determine the roughness of the films. The crystal phase of Cu oxide thin films was investigated by X-ray diffraction (XRD, PHILIPS X'Pert-MPD, Netherlands) with Cu Kα radiation in normal mode. The chemical analyses of Cu oxide thin films were carried with X-ray photoelectron spectroscopy (XPS, VG MultiLab 2000, UK). The applied X-ray source was monochromatic Al Kα (1486.6 eV) source with a power of 24 kW and a beam current of 16.5 mA. The base pressure of XPS chamber was maintained at 1×10^{-10} Torr by pumping with a rotary vane pump, a turbo molecular pump, and an ion pump. The detailed parameters for XPS analysis are described elsewhere.[22] High resolution XP spectra of Cu 2p and O 1s region were collected with a pass energy of 20 eV, a dwell time of 50 ms, and an energy step sized of 0.05 eV. The binding energy of each spectrum was corrected by aliphatic C 1s at 284.6 eV as a reference.[23] The water contact angles of Cu oxide thin films were carried with a customized contact angle analyzer to investigate the hydrophilicity of Cu oxide films with 0.2 μL water droplet. The measurement of contact angle was performed in static contact mode and the contact angle of obtained image was determined by Motic images analysis program (ver. 2.0).

Results and Discussion

The thickness of Cu oxide thin films was measured by SEM images. Figure 1 shows cross-sectional views of Cu-rt, Cu-100, Cu-200, and Cu-300, respectively. The sample notation used here such as Cu-300 means that the annealing temperature was 300 °C during Cu oxide deposition. As shown in Figure 1, the thickness of thin films is relatively constant about 180 nm and the columnar structure was grown normal to the Si surface. The thickness measured using SE analysis is listed in Table 1 for comparison. There is a slight discrepancy between the thicknesses obtained by SEM and SE. This caused because the thickness measured from the SEM images was ambiguous due to the surface roughness. The relatively constant film thickness caused by the constant mixing ratio of sputter gas. The film thickness was not affected by the annealing temperature carried in this study.

The crystal structure of Cu oxide films was characterized

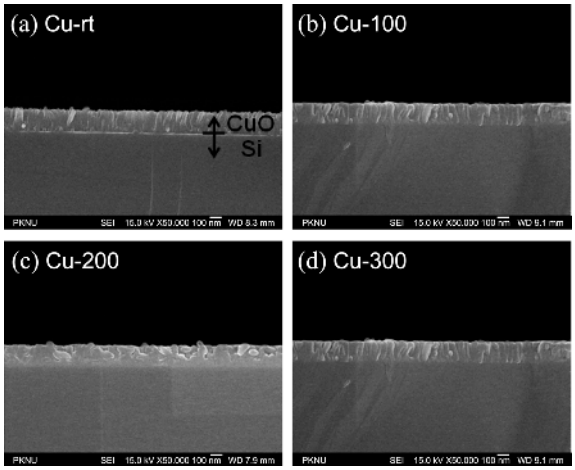

Figure 1. The cross-sectional SEM images of Cu oxide thin films obtained at different annealing temperatures: (a) Cu-rt, (b) Cu-100, (c) Cu-200, and (d) Cu-300.

Table 1. The parameters of Cu oxide films obtained at different substrate temperatures

	Cu-rt	Cu-100	Cu-200	Cu-300
Thickness (nm), SE	154.8	176.1	189.9	183.6
d-spacing (Å), XRD	2.544	2.538	2.533	2.527
Grain size (nm), AFM	44.9	55.5	70.1	89.6
Band gap (eV), SE	2.35	2.99	3.06	2.85

by XRD and shown in Figure 2. The diffraction peaks of Cu oxide films were matched with the monoclinic CuO[24] and the Si peak was detected at about 69° (not shown here). The characteristic diffraction peaks of CuO of (110), $(\bar{1}11)/(002)$,

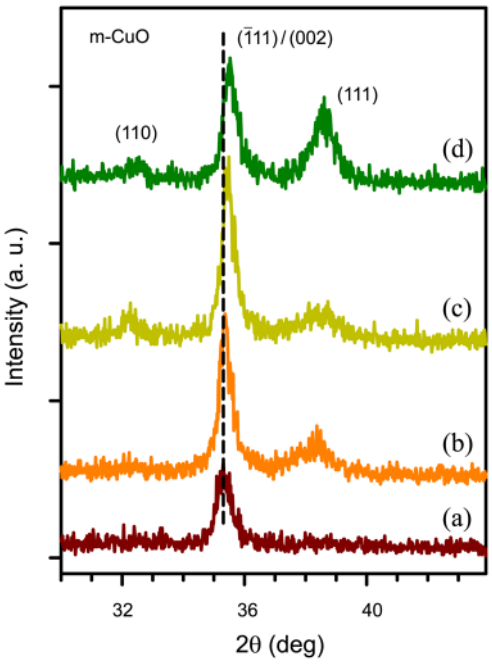

Figure 2. XRD patterns of the Cu oxide thin films as a function of annealing temperature: (a) Cu-rt, (b) Cu-100, (c) Cu-200, and (d) Cu-300.

and (111) phases were observed. All the Cu oxide films obtained at different annealing temperatures possessed relatively weaker intensity of (110) than other phases. The intensity of $(\bar{1}11)/(002)$ phase was increased up to 200 °C and then decreased with high preference. The peak intensity of (111) phase was increased at 300 °C. It could be certain that the preferential growth of CuO changed from $(\bar{1}11)/(002)$ to (111) phase above 200 °C of annealing temperature. It is interesting to note that the $(\bar{1}11)/(002)$ peak position shifted to higher Bragg diffraction angle by annealing. It indicates that CuO crystals formed more packed crystal by highly mobile active species and have a smaller lattice parameter summarized in Table 1. The crystal size of CuO was calculated using the Scherrer's equation to verify the crystal size of the thin films. The crystal sizes obtained from $(\bar{1}11)/(002)$ peak were 13.74, 16.77, 16.79, and 16.45 nm for Cu-rt, Cu-100, Cu-200, and Cu-300, respectively. The thermal energy produced by annealing led enhancement of mobility of active species and formed more packed and larger crystalline films. This phenomenon was observed in microwave dielectric ceramic thin films by Shi *et al.*.[25] The results of the investigation of the polycrystalline Cu oxide films annealed below 600 °C were reported that the polycrystalline phases were converted to single crystalline or continuously existed mixing phases of Cu_2O and CuO.[20,26,27] According to the equilibrium phase diagram of the Cu-O system, CuO is the stable phase up to 300 °C even at low oxygen partial pressure.[28] Therefore the formation of CuO phase was reasonable and the annealing temperature affected on the crystal quality, not the crystal phase in Cu oxide thin films synthesized by r.f. magnetron sputtering. The kinds of crystal structure were not affected but the preferential orientation was affected by annealing temperature.

Figure 3 shows AFM images and the roughness (rms) values of Cu oxide films. The surface roughness of thin films is equal to the half of the peak to the valley height.[29] The average grain sizes of Cu oxide thin films are summarized in Table 1. The grain size increased as the annealing temperature increased. This can be explained by the thermal energy being supplied by annealing used for filling the micro-voids or defects among columnar structures by active species. So the grain size increased by annealing and this caused the increase of roughness. This phenomenon shows agreement with the previous study about the relationship between roughness and grain growth.[30,31]

The chemical analysis, which extensively focused on the oxidation state of elements, was performed by XPS. The high resolution Cu 2p XP spectra are shown in Figure 4(a) and the representative deconvoluted Cu $2p_{3/2}$ peaks for Cu-rt and Cu-300 are shown in Figures 4(b) and (c), respectively. The XP spectra of Cu 2p showed characteristic doublet peaks with 20 eV of SOS (spin obit splitting) and the shake-up satellite peaks were observed at about 7 and 9 eV of binding energies higher than that of Cu 2p peak.[32] The satellite peaks indicate the formation of CuO.[33] These results are cross matched with the results of XRD. The Cu $2p_{3/2}$ peaks were curve fitted with three species corresponding to Cu_2O (933.20 eV, FWHM: 1.56 eV), CuO (934.34 eV, FWHM: 1.56 eV) and $Cu(OH)_2$ (935.61 eV, FWHM: 1.67 eV).[28,34] As shown in Figure 4(a), no significant difference was detected in the Cu 2p XP spectra of Cu oxide films. As mentioned previously, only the crystalline CuO peak was detected for the Cu oxide films in XRD study however the coexistence of CuO and Cu_2O was confirmed by XPS investigation. From the above observation, it may be concluded that Cu_2O existed as an amorphous phase and CuO preferential growth in monoclinic crystal phase. In addition, the oxidation of Cu was almost independent of the annealing temperature and Cu_2O and CuO coexisted with constant mixing ratio (Figures 4(b) and (c)). In the high resolution XP spectra of O 1s region (Figure 5), the deconvoluted O 1s peaks were assigned for three species, O-Cu bond (529.56 eV, FWHM: 0.95 eV), O-C bond (531.07 eV, FWHM: 1.17

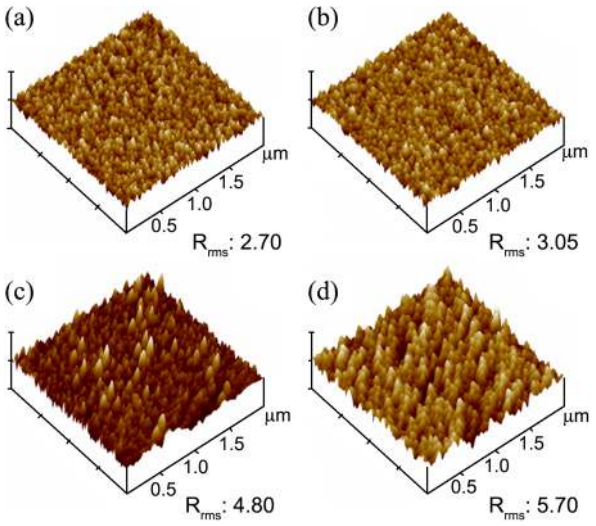

Figure 3. AFM images of Cu oxide thin films deposited with different annealing temperature at (a) rt, (b) 100, (c) 200, and (d) 300 °C. X scale is 2 μm and Z scale is 40 nm for the images. The surface roughness (R_{rms}) was 2.70, 3.05, 4.80, and 5.70 nm in rms of (a), (b), (c), and (d), respectively.

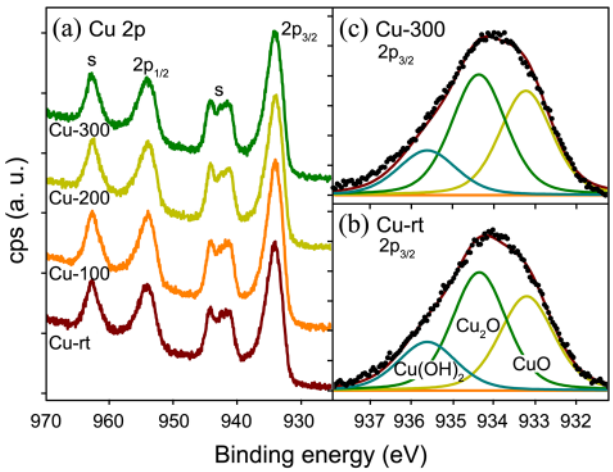

Figure 4. (a) High resolution XP spectra of Cu 2p with different annealing temperatures, s means the satellite shake up peak of CuO. (b) The deconvoluted spectra of Cu $2p_{3/2}$ of Cu-rt and (c) Cu-300.

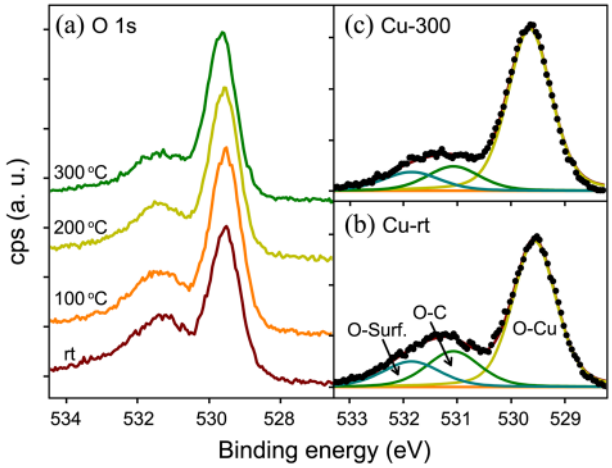

Figure 5. (a) High resolution XP spectra of O 1s with different annealing temperatures. (b) The deconvoluted spectra of O 1s at rt and (c) at 300 °C.

eV) and surface oxygen (531.85 eV, FWHM: 1.27 eV) from lower to higher binding energy (Figures 5(b) and (c)). Even though the deposition was carried in high vacuum condition, the residual carbon contaminants in the deposition chamber were attributed to the formation of carbonyl species.[35] The third species, surface oxygen, indicated that hydroxide species caused by the residual hydrogen species such as water in the deposition chamber and adsorbed on the surface to form $Cu(OH)_2$.[36] The ratio of $Cu(OH)_2$ calculated from O 1s XP spectra decreased with an increase in the annealing temperature and it is consistent with the result of Cu 2p XP spectra. This means that the ratio of Cu oxide increased as the annealing temperature increased and the transformation

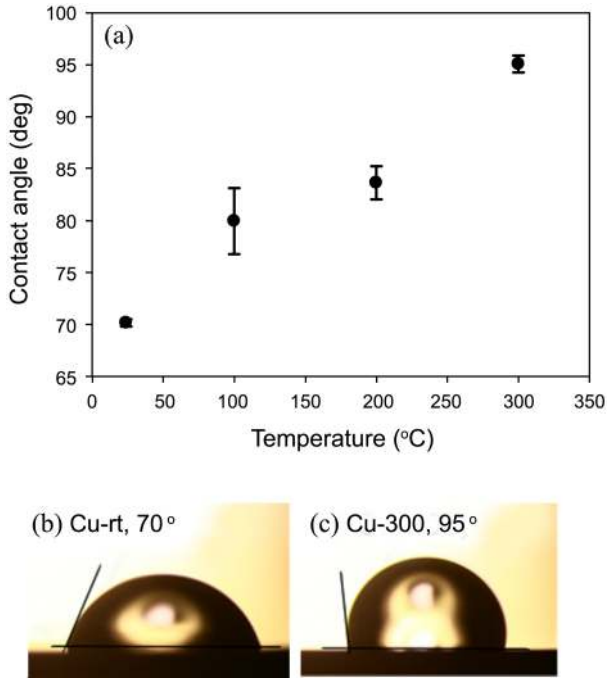

Figure 6. (a) Variation of contact angle as a function of different annealing temperatures. The images of contact angle measurement for Cu-rt in (b) and Cu-300 in (c).

between Cu_2O and CuO was undetectable.

The contact angles of Cu oxide thin films were measured to check hydrophilicity of the Cu oxide films and shown in Figure 6(a) and the representative images for Cu-rt and Cu-300 are shown in Figures 6(b) and (c). Cu oxide thin films obtained at high annealing temperature have more hydrophobic surface than that obtained at low temperature, confirmed by the higher degree of the contact angle of water against the Cu oxide films. This observation is opposite with the common Wenzel's model[37] which is good model for homogeneous wetting surface, the contact angle decreased as the roughness of the surface increased. The Cu oxide films in this study, however, showed opposite propensity. This could be explained by lotus effect[38]; the surface wettability is changed from hydrophilic to hydrophobic as the roughness increased. The wettability is attributed to the composition and roughness of the surface. From the XPS results, the composition of Cu oxide thin films was not the major factor. Therefore the contact angle in this study was affected by the surface roughness and grain size. According to the AFM and SE results, the roughness increased as a function of annealing temperature. As a result, the contact angle was significantly dependent on the annealing temperature.

To estimate optical band gap of the Cu oxide thin films, the absorption coefficient (α) was plotted against the photon energy. The direct band gap, shown in Figure 7, was determined by the x-intercept of the extrapolating line of linear portion which is associated to the Urach tail near the band edge.[39] The detailed information to calculate the band gap was described elsewhere.[40] The obtained direct band gap values showed the blue shift up to 200 °C and then red shift was observed. This phenomenon was also reported in Cu oxide thin films deposited by thermal oxidation of metallic Cu films between 100 and 450 °C.[20] The optical band gap was determined by several parameters such as the grain growth, crystallinity, and stress of the films. It is well known that the increase of grain size could cause the red shift.[39] In this study, the grain size of Cu oxide films monotonically

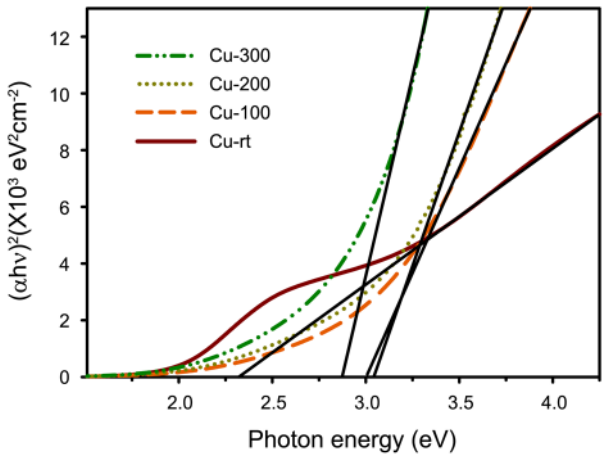

Figure 7. Plots of $(\alpha h\nu)^2$ versus photon energy of the Cu oxide films under various substrate temperatures. The tangent lines were calculated from the data points.

increased with increasing the annealing temperature from AFM result. So this implies that the grain size was not the dominant factor to change the direct band gap. To understand the effect of crystallinity on the direct band gap changing phenomenon, the physical model of the Cu oxide thin films should be considered. All samples have monoclinic CuO and amorphous CuO_2 and $Cu(OH)_2$. This propensity of the band gap change, blue shift then red shift, is the same as the intensity change of $(\bar{1}11)/(002)$ peak of monoclinic CuO. The intensity of $(\bar{1}11)/(002)$ increased with increasing the annealing temperature up to 200 °C then decreased at 300 °C. In order to verify the final factor, stress, it is reported that the stress was decreased with increasing the film thickness.[41] In this study, the thickness of Cu oxide thin films analyzed by SE data was slightly increased up to 200 °C and then decreased at 300 °C (Table 1). It is helpful to think that the stress of the films decreased and then increased at 300 °C. If the shift of the direct band gap was attributed to the stress in the Cu oxide thin films, the band gap should be red shifted then blue shifted. However, our band gap measurement shows opposite propensity with the film thickness. So we can conclude the band gap shift is strongly affected by the preferential growth in $(\bar{1}11)/(002)$ phase. We should note the $(\alpha h\nu)^2$ values at about 2.5 eV of photon energy on Cu-rt sample. This may caused by lack of perfectness of the Cu oxide films or more than one direct band gap states exist in the Cu oxide sample.

Conclusion

The Cu oxide thin films were synthesized by reactive r.f. magnetron sputtering from metallic Cu target. During the deposition process, the sputter gas mixing ratio maintained constant, but the annealing temperature increased from rt to 300 °C. According to the XRD and XPS results, the Cu oxide films consist of monoclinic CuO and amorphous Cu_2O and $Cu(OH)_2$. The phases of Cu oxide were not affected by annealing temperature, while the roughness of films increased with an increase in the annealing temperature. The crystal size and contact angle increased, as the annealing temperature increased. The increase of the roughness dependent on the grain growth. The hydrophobic character of the Cu oxide films was detected by an increase of annealing temperature . The direct band gap shift was observed initiating blue shift up to 200 °C and then red shift.

Acknowledgments. This research was supported by Basic Science Research Program through the National Research Foundation of Korea (NRF) funded by the Ministry of Education, Science and Technology (2010-0021332).

References

1. Nakano, Y.; Saeki, S.; Morikawa, T. *Appl. Phys. Lett.* **2009**, *94*, 022111.
2. Kbayashi, H.; Nakamura, T.; Takahashi, N. *Mater. Chem. Phys.* **2007**, *106*, 292.
3. Ray, S. C. *Sol. Energy Mater. Sol. Cells* **2001**, *68*, 307.
4. Oral, A. Y.; Menşur, E.; Aslan, M. H.; Başaran, E. *Mater. Chem. Phys.* **2004**, *83*, 140.
5. Lu, H.-C.; Chu, C.-L.; Lai, C.-Y.; Wang, Y.-H. *Thin Solid Films* **2009**, *517*, 4408.
6. Hoa, N. D.; An, S. Y.; Dung, N. Q;. Quy, N. V.; Kim, D. *Sens. Actuators B* **2010**, *148*, 239.
7. Barreca, D.; Comini, E.; Gasparotto, A.; Maccato, C.; Sada, C.; Sberveglieri, G.; Tondello, E. *Sens. Actuators, B* **2009**, *141*, 270.
8. Medina-Valtierra, J.; Ramírez-Oriz, J.; Arroyo-Rojas, V. M.; Ruiz, F. *Appl. Catal. A* **2003**, *238*, 1.
9. Wong, L. M.; Chiam, S. Y.; Huang, J. Q.; Wang, S. J.; Pan, J. S.; Chim, W. K. *J. Appl. Phys.* **2010**, *108*, 033702.
10. Mahalingam, T.; Chitra, J. S. P.; Chu, J. P.; Moon, H.; Kwon, H. J.; Kim, Y. D. *J. Mater. Sci.: Mater. Electron.* **2006**, *17*, 519.
11. Fernando, C. A. N.; Bandara, T. M. W. J.; Wethasingha, S. K. *Sol. Energy Mater. Sol. Cells* **2001**, *70*, 121.
12. Ristova, M.; Neskovska, R.; Mirceski,V. *Sol. Energy Mater. Sol. Cells* **2007**, *91*, 1361.
13. Markworth, P. R.; Liu, X.; Dai, J. Y.; Fan, W.; Marks, T. J.; Chang, R. P. H. *J. Mater. Res.* **2001**, *16*, 2408.
14. Golden, T. D.; Shumsky, M. G.; Zhou, U.; Vander Werf, R. A.; Van Leeuwen, R. A.; Switzer, J. A. *Chem. Mater.* **1996**, *8*, 2499.
15. Özer, N.; Tepehan, F. *Sol. Energy Mater. Sol. Cells* **1993**, *30*, 13.
16. Ray, S. C. *Sol. Energy Mater. Sol. Cells* **2001**, *68*, 307.
17. Kosugi, T.; Kaneko, S. *J. Am. Chem. Soc.* **2004**, *81*, 3117.
18. Chen, A.; Long, H.; Li, X.; Li, Y.; Yang, G.; Lu, P. *Vacuum* **2009**, *83*, 927.
19. Ma, X.; Wang, G.; Yukimura, K.; Sun, M. *Surf. Coat. Technol.* **2007**, *201*, 6712.
20. Figueiredo, V.; Elangovan, E.; Gonçalves, G.; Barquinha, P.; Pereira, L.; Franco, N.; Alves, E.; Martins, R.; Fortunato, E. *Appl. Surf. Sci.* **2008**, *254*, 3949.
21. Ogwu, A. A.; Bouquerel, E.; Ademosu, O.; Moh, S.; Crossan, E.; Placido, F. *J. Phys. D: Appl. Phys.* **2005**, *38*, 266.
22. Park, J. Y.; Heo, J. K.; Kang, Y. C. *Bull. Korean Chem. Soc.* **2010**, *31*, 397.
23. Kang, Y. C.; Khanal, R.; Park, J. Y.; Ramsier, R. D.; Khatri, H.; Marsillac, S. *J. Vac. Sci. Technol., B* **2010**, *28*, 545.
24. JCPDS Database, International Center for Diffraction Data. 2003, PDF 80-1917.
25. Shi, F.; Cui, C. *Inorg. Mater.* **2010**, *46*, 565.
26. Yoon, K. H.; Choi, W. J.; Kang, D. H. *Thin Solid Films* **2000**, *372*, 250.
27. Papadimitropoulos, G.; Vourdas, N.; Davazoglou, V. Em.; Vamvakas, D. *Thin Solid Films* **2006**, *515*, 2428.
28. Al-Kuhaili, M. F. *Vacuum* **2008**, *82*, 623.
29. Petrik, P.; Biró, L. P.; Fried, M.; Lohner, T.; Berger, R.; Schneider, C.; Gyulai, J.; Ryssel, H. *Thin Solid Films* **1998**, *315*, 186.
30. Venkataraj, S.; Kappertz, O;. Liesch, Ch.; Detemple, R.; Jayavel, R.; Wuttig, M. *Vacuum* **2004**, *75*, 7.
31. Mohamed, S. H.; Venkataraj, S. *Vacuum* **2007**, *81*, 636.
32. Wagner, C. D.; Riggs, W. M.; Davis, L. E.; Moulder, J. F.; Muilenberg, G. E. *Handbook of X-ray Photoelectron Spectroscopy*; Perkin-Elmer Corp.: 1979; p 82.
33. Chusuei, C. C.; Brookshier, M. A.; Goodman, D. W. *Langmuir* **1996**, *15*, 2806.
34. Morales, J.; Sánchez, L.; Martín, F.; Ramos-Barrado, J. R.; Sánchez, M. *Thin Solid Films* **2005**, *474*, 133.
35. Miyamura, T.; Koike, J. *Mater. Sci. Eng. A* **2007**, *445-446*, 620.
36. Wong, L. M.; Chiam, S. Y.; Huang, J. Q.; Wang, S. J.; Pan, J. S.; Chim, W. K. *J. Appl. Phys.* **2010**, *108*, 033702.
37. Marmur, A. *Langmuir* **2003**, *19*, 8343.
38. Lin, F.; Zhang, Y.; Xi, J.; Zhu, Y.; Wang, N.; Xia, F.; Jiang, L. *Langmuir* **2008**, *24*, 4114.
39. Zhang, J. P.; Zhang, L. D.; Zhu, L. Q.; Zhang, Y.; Liu, M.; Wang, X. J. *J. Appl. Phys.* **2007**, *102*, 114903.
40. Bihn, J. H.; Park, J. Y.; Kang, Y. C. *J. Korean. Phys. Soc.* in print.
41. Roy, S. C.; Sharma, G. L.; Bhatnagar, M. C. *Solid State Commun.* **2007**, *141*, 243.